Published in final edited form as:
Nat Neurosci. 2015 January ; 18(1): 87–96. doi:10.1038/nn.3890.

Early *depolarizing* GABA controls critical period plasticity in the rat visual cortex

Gabriele Deidda[1,#], **Manuela Allegra**[2,3,#], **Chiara Cerri**[3], **Shovan Naskar**[1], **Guillaume Bony**[1], **Giulia Zunino**[4], **Yuri Bozzi**[3,4], **Matteo Caleo**[3,*], and **Laura Cancedda**[1,*]

[1]Neuroscience and Brain Technologies Department, Istituto Italiano di Tecnologia, via Morego, 30, 16163 Genova.

[2]Scuola Normale Superiore, Pisa, Italy

[3]CNR Neuroscience Institute, Pisa, Italy

[4]Centre for Integrative Biology (CIBIO), Trento, Italy

SUMMARY

Hyperpolarizing and inhibitory GABA regulates “critical periods” for plasticity in sensory cortices. Here, we examine the role of early, depolarizing GABA in controlling plasticity mechanisms. We report that brief interference with depolarizing GABA during early development prolonged critical period plasticity in visual cortical circuits, without affecting overall development of the visual system. The effects on plasticity were accompanied by dampened inhibitory neurotransmission, down-regulation of BDNF expression, and reduced density of extracellular matrix-perineuronal nets. Early interference with depolarizing GABA decreased perinatal BDNF signaling, and pharmacological increase of BDNF signaling during GABA interference rescued the effects on plasticity and its regulators later in life. We conclude that depolarizing GABA exerts a long-lasting, selective modulation of plasticity of cortical circuits by a strong crosstalk with BDNF.

INTRODUCTION

Sensory systems are immature at birth and undergo experience-dependent maturation during development. In particular, during a critical period (CP) of postnatal development, neuronal circuits are plastic and easily shaped by sensory experience to reach the mature structural

Corresponding author:laura.cancedda@iit.it.

AUTHOR’S CONTRIBUTIONS G.D. performed *in vitro* electrophysiological recordings, Western blot experiments, *in utero* electroporation, immunohistochemistry and wrote the manuscript. M.A. performed *in vivo* electrophysiological recordings, Western blot experiments, immunohistochemistry, behavioral testing, retino-geniculate axons labeling and wrote the manuscript. C.C. contributed to *in vivo* electrophysiological recordings. G.B. and S.N. performed patch-clamp experiments. G.Z. and Y.B. performed RT-PCR and immunohistochemistry. M.C. and L.C. designed the experiments and wrote the manuscript. M.C., Y.B. and L.C. provided financial support. All authors read and revised the manuscript.

[#]Equal contribution as first authors

[*]Equal contribution as senior authors

Laura Cancedda is co-author on provisional application number US: 61/919,195, 2013

A Supplementary methods checklist is available.

and functional features of the adult [1-2]. In the visual system, experience strongly regulates the maturation of basic properties of the visual cortex (e.g., visual acuity), as well as both the opening and closure of the CP [3-4]. Hyperpolarizing and inhibitory γ-aminobutyric acid (GABA) signaling through Cl^--permeable ionotropic $GABA_A$ receptors is critical for experience-dependent development and plasticity of the visual cortex [2, 5-7]. Nevertheless, GABA exerts a depolarizing and mainly excitatory action during early development (until the first/second postnatal week in rodents) [8-9]. Indeed, immature neurons accumulate Clintracellularly *via* the Na^+-K^+-$2Cl^-$ (NKCC1) cotransporter, resulting in a net depolarizing efflux of Cl^- ions upon $GABA_A$ receptor opening. Conversely, in adolescent and adult animals, cotransporter K^+-$2Cl^-$ (KCC2) is mostly expressed, lowering the intracellular Cl-concentration $[Cl]_i$ and converting $GABA_A$ergic transmission to inhibitory.

Although *hyperpolarizing* and inhibitory GABAergic transmission is a well-known regulator of visual system development and plasticity, and *depolarizing* GABAergic signaling is fundamental for early physiological maturation of various brain areas [10], nothing is known about the role of *depolarizing* GABA in the regulation of cortical plasticity. Here, we found that brief interference with depolarizing GABA during early postnatal development prolongs the CP of plasticity in the visual cortex, without affecting the overall development of the visual system. This effect is accompanied by changes in fundamental regulators of plasticity and it is rescued by increasing BDNF signaling during depolarizing-GABA interference.

RESULTS

Early depolarizing GABA controls CP plasticity

To hamper depolarizing $GABA_A$ signaling, we treated rat pups with the NKCC1-inhibitor bumetanide (i.p., 0.2 mg/Kg, twice a day because of its pharmacokinetics [11]) from postnatal day (P) 3 to P8 (Fig. 1a), when NKCC1 is the main K^+-Cl^- cotransporter in the cerebral cortex (Supplementary Fig. 1) [8-10]. Indeed, bumetanide crosses the brain-blood barrier [11] and effectively shifts the reversal potential of GABA (E_{GABA}), converting $GABA_A$ signaling to hyperpolarizing in young rats [10, 12-13].

To assess whether the perinatal interference with depolarizing GABA impacted the time-course of the CP for visual cortex plasticity, we used a classical paradigm of experience-dependent plasticity (i.e., 3 days of monocular deprivation, MD) in bumetanide- and vehicle-treated rats (Fig. 1a). When performed during the CP (but not in the adult), brief MD results in a dramatic shift of ocular dominance (OD) of cortical neurons in favor of the non-deprived eye [14]. To define the time course of the sensitive period for plasticity, we performed MD experiments at different ages, spanning its normal opening and closing [15]. To quantify the OD shift, we performed *in vivo* electrophysiological recordings, and measured the contralateral-to-ipsilateral (C/I) visual-evoked potentials (VEP) ratio (i.e., the ratio of VEP amplitudes recorded by stimulating the contralateral or ipsilateral eye) in bumetanide- and vehicle-treated animals, either monocularly deprived (MD) or left un-deprived (nonMD). Baseline binocularity was comparable between nonMD bumetanide- and vehicle-treated animals at all tested ages (C/I VEP ratio 1.5 - 2 for both groups; Fig. 1c–h), indicating no specific effect of early bumetanide treatment on general development of binocularity. On the other hand, the MD experiments indicated that while the onset of CP

plasticity was unaffected by bumetanide treatment, its closure was significantly delayed (Fig. 1b). Indeed, OD plasticity rose similarly from P17 to P20 and it was maximal at P26 in both bumetanideand vehicle-treated rats (Fig. 1c–e). Conversely, at P35, consistent and significant OD plasticity could be induced only in bumetanide-treated animals (Fig. 1b,f). Interestingly, the shift in eye preference of bumetanide-treated animals following MD at P35 involved a depression of responses driven by the deprived eye, an effect typical of juvenile-like plasticity [16] (Supplementary Fig. 2). The CP was over in both groups by P45 and P75 (Fig. 1b,g,h).

To strengthen the *in vivo* data, we assessed the level of *in vitro* plasticity in the visual system of animals previously treated with bumetanide or vehicle. In particular, we performed field-potential recordings in acute visual cortical slices to assess long-term potentiation of layer II/III synaptic responses by theta burst stimulation (TBS) of the white matter (WM-LTP). This is a classical *in vitro* model of visual cortical plasticity known to undergo an age-dependent developmental decline that closely correlates with the developmental decline of the susceptibility to MD *in vivo* [1, 3, 5]. Consistent with MD experiments, we found that early GABAergic interference prolonged the CP for WM-LTP induction (Fig. 2a). This is exemplified in Fig. 2b–g, which shows the average time course of field potential responses before and after TBS at different ages. Whereas both bumetanide- and vehicle-treated animals opened the CP after P17 and showed maximal plasticity at P20-P26 (Fig. 2a–d), only bumetanide-treated animals showed significant WM-LTP at P35 (Fig. 2a,e). Conversely, both experimental groups did not show significant plasticity at older ages (P45 and P75; Fig. 2a,f,g). Altogether, these results indicate that interfering with depolarizing GABA during early development significantly extends the sensitive period for activity-dependent rearrangements of cortical circuits later in life.

Early bumetanide treatment does not affect overall anatomy

To exclude the possibility that the effect on plasticity was due to defects in anatomical development of the visual system [10, 17], we investigated segregation of eye-specific inputs in the dorsal lateral geniculate nucleus (dLGN), and migration/morphological maturation in the visual cortex of animals perinatally treated with bumetanide or vehicle, since these processes occur early in rat perinatal life [17-18]. To visualize retinal afferents from both eyes, we performed intravitreal injections of cholera toxin beta (CTB) fragment conjugates of different colors and analyzed coronal dLGN sections at P35 (Fig. 3a). We found clear segregation of fibers from the two eyes in both bumetanide- and vehicle-treated rats (Fig. 3b), indicating a normal development of retino-geniculate projections.

To investigate the structural development of the visual cortex, we performed *in utero* electroporation of progenitors of excitatory neurons committed to layer II/III with a plasmid encoding for enhanced green fluorescent protein (EGFP) at embryonic day 17.5 (E17.5; Fig. 3c). This allowed visualization of neuronal migration and morphological maturation of the neuronal progeny of transfected cells by imaging EGFP fluorescence. We found that all EGFP-positive neurons reached layer II/III both in bumetanide- and vehicle-treated animals at P35 (Fig. 3d). Moreover, morphological reconstruction of EGFP-positive neurons did not reveal any significant difference in morphological maturation between the two groups (Fig.

3d and Supplementary Fig. 3). Next, to assess the development of GABAergic interneurons, we examined their laminar distribution by immunostaining for the GABA biosynthetic enzyme GAD67 in cortical sections from bumetanide- and vehicle-treated rats at P35. We found no significant differences in the distribution of interneurons between the two groups (Fig. 3e,f).

Early bumetanide treatment does not affect visual function

Next, we investigated whether bumetanide treatment could instead affect the overall development of the visual system at the functional level. In general, bumetanide-treated animals developed normally, as their gain of body weight and timing of eye opening were comparable to controls (Supplementary Fig. 4 and Fig. 4a). Moreover, bumetanide- and vehicle-injected animals performed equally in learning a visual discrimination task (Prusky visual water box; Fig. 4b). Using the same test, we measured visual acuity longitudinally [3] starting from P24, and we found no deficits in its maturation in bumetanide-treated animals (Fig. 4c). Finally, we measured basic physiological parameters in primary visual cortex by VEP recordings at P35 (i.e., when they are completely mature) [19]. We found that spatial resolution (visual acuity), contrast threshold, VEP amplitude and latency in bumetanide-treated rats were within the normal range and did not differ from controls (Fig. 4d–g). Thus, briefly interfering with depolarizing GABA during early development prolongs the CP for OD plasticity and WM-LTP into adulthood, without affecting basic anatomical and physiological development of the visual system.

Bumetanide effects are not due to regulation of osmolarity

To ensure that the effects on visual cortical plasticity upon bumetanide treatment were specifically due to regulation of NKCC1 rather than to side effects of the pharmacological treatment, we treated rat pups perinatally (P3-P8) with another NKCC1 inhibitor (furosemide; i.p., 20 mg/Kg, twice a day), and addressed the level of plasticity at P35. In fact, furosemide blocks both NKCC1 and KCC2. Nevertheless, due to the low expression of KCC2 at the age of treatment (Supplementary Fig. 1), furosemide would mimic the effect of the specific NKCC1-blocker bumetanide on chloride regulation under our experimental conditions. Accordingly, we found that furosemide-treated animals displayed higher levels of plasticity than vehicle-treated controls at P35, as they responded to brief MD with a robust OD shift and displayed significant WM-LTP in slices (Fig. 5ab). These plastic changes were perfectly comparable to those observed in bumetanide-injected rats (Fig. 5a,b), indicating the involvement of early chloride homeostasis in regulating plasticity later in life.

Nevertheless, direct regulation of NKCC1 also results in neuronal shrinkage, as bumetanide and furosemide are FDA-approved diuretics that regulate blood osmolarity [20] (Fig. 5c). Thus, we verified that the effect of bumetanide and furosemide on cortical plasticity not be simply due to an alteration in the volume of the extracellular space [21]. To this aim, we treated rat pups perinatally (P3-P8) with the osmotic diuretic mannitol (i.p., 7.5 g/Kg) [20, 22], which regulates the extracellular-space volume without affecting NKCC1 activity [20, 22]. Mannitol-treated animals displayed the same levels of plasticity as vehicle-treated controls,

both *in vivo* and *in vitro* (Fig. 5a,b), indicating that bumetanide and furosemide regulate cortical plasticity *via* modulation of Cl^- homeostasis, but not cell volume.

Variations in CP regulators accompany bumetanide effects

Next, we investigated possible mechanisms responsible for the higher levels of plasticity found at P35 in bumetanide-treated animals. First, as inhibitory GABAergic transmission is a major regulator of the closure of the CP [5, 7], we examined basal GABAergic transmission in visual cortical slices from P35 animals perinatally treated with bumetanide or vehicle by means of whole-cell patch-clamp recordings. While basic membrane properties (membrane resistance, membrane capacitance, and membrane resting potential) of layer II/III visual cortical neurons were comparable in the two experimental groups (Supplementary Fig. 5a–c), the frequency of miniature inhibitory postsynaptic currents (mIPSCs) was drastically reduced in bumetanide-treated animals (bumetanide, 0.26 ± 0.05 Hz *vs* vehicle, 0.62 ± 0.16 Hz; Fig. 6a). Conversely, there was no difference in the amplitude (Fig. 6b) or the kinetics (tau and rise time; Supplementary Fig. 5d,e) of these events. Interestingly, we found no significant effect of perinatal bumetanide treatment on the frequency of miniature excitatory AMPA postsynaptic currents at P35 (bumetanide 1.40 ± 0.37 Hz, n = 10 cells, *vs* vehicle 1.79 ± 0.41 Hz, n = 9 cells; Student's *t*-test, $P = 0.501$). Thus, we investigated whether we could rescue the persistent OD plasticity of bumetanide-treated animals at P35 by enhancing GABA ergic transmission with i.p. injection of diazepam [23-24] A during the period of MD in a group of rats perinatally treated with bumetanide (Supplementary Fig. 6a). We found that the OD shift was significantly mitigated by diazepam infusion (Supplementary Fig. 6b), indicating that a reduced inhibitory tone partly accounts for the effect of bumetanide on plasticity at P35, and that other regulators of plasticity may also play a significant role.

Thus, as brain-derived neurotrophic factor (BDNF) controls the closure of the CP in the visual system by influencing inhibitory circuits [5, 14], we investigated its expression in bumetanide- and vehicle-treated animals at P35. By Western blot experiments, we found significantly lower levels of BDNF in visual cortices from bumetanide-treated animals (Fig. 6c).

Finally, components of the extracellular matrix such as chondroitin sulphate proteoglycans (CSPGs) also limit experience-dependent plasticity by condensing mostly around parvalbumin (PV)-positive interneurons in the form of perineuronal nets (PNNs) [14, 19, 25]. Therefore, we investigated whether early bumetanide-treatment affected PNN development around PV cells by performing immunostaining using *Wisteria floribunda* lectin (WFA, to label CSPG glycosaminoglycan chains) and an antibody for PV at P35 (Fig. 6d, red and green, respectively). Visual cortical slices derived from bumetanide-treated animals showed a lower PNN density compared to controls (Fig. 6d,e). Interestingly, there was no significant difference in the absolute number of PV-positive cells (Fig. e), and in the density of PV-positive boutons onto pyramidal neurons in bumetanide- and vehicle-treated rats (Supplementary Fig. 7). Nevertheless, double labeling for WFA and PV confirmed that a lower proportion of PV-positive interneurons were surrounded by PNNs in bumetanide-treated animals (Fig. 6d,e).

Altogether, these findings indicate that the increased plasticity in bumetanide-treated animals at P35 is accompanied by modulation of well-known “plasticity brakes” such as GABAergic inhibitory neurotransmission, BDNF and perineuronal nets [4].

If release of the plasticity brakes were responsible for the higher degree of plasticity in bumetanide-treated animals at P35, then one would expect no difference in the levels of these same plasticity brakes at ages when the potential for plasticity is comparable between bumetanide- and vehicle-treated animals. Therefore, we assessed mIPSCs and BDNF levels at P26 (the peak of plasticity for both bumetanide- and vehicle-treated animals) and mIPSCs, PNNs, and BDNF levels at P75 (when the CP is over in both groups). Recordings at P26 and P75 showed indeed no differences in either frequency or amplitude of mIPSCs between bumetanide- and vehicle-treated animals (Supplementary Fig. 8a,b and 9a,b). The frequency of miniature excitatory AMPA postsynaptic currents was also superimposable between the groups (P26, bumetanide 1.22 ± 0.26 Hz, n = 6 cells, *vs* vehicle 1.36 ± 0.20 Hz, n = 9 cells; Student’s *t*-test, $P = 0.671$; P75, bumetanide 0.87 ± 0.22 Hz, n = 7 cells, *vs* vehicle 1.05 ± 0.29 Hz, n = 9 cells; Student’s *t*-test, $P = 0.644$). In keeping with the data on mIPSCs, we found comparable levels of BDNF at P26 and P75 in bumetanide- and vehicle-treated animals (Supplementary Fig. 8c and 9c). The density of PNNs was assessed at P75, and again we found no significant changes in bumetanide-treated animals (Supplementary Fig. 9d).

Early DHF co-treatment rescues bumetanide effects at P35

What are the possible mechanisms that link the effect of early treatment with bumetanide to the prolongation of CP plasticity? Depolarizing GABA and BDNF are involved in a positive feedback reciprocal regulation during early development [26-27]. In particular, activation of $GABA_A$ receptors triggers augmented release of BDNF and enhanced phosphorylation of its receptor TrkB, that in turn reduces internalization of $GABA_A$ receptors from the plasma membrane [26]. Therefore, we hypothesized that perinatal bumetanide treatment may disrupt the positive loop described above, thus reducing BDNF signaling in response to $GABA_A$ receptor activation. To test this hypothesis, we collected visual cortex samples from pups perinatally treated with bumetanide or vehicle (P3-P8) and systemically challenged at P8 by acute injection of a $GABA_A$ receptor agonist (midazolam; i.p., 5 mg/Kg; Fig. 7a). By quantitative RT-PCR, we found a significant upregulation of *Bdnf* mRNA expression in vehicle-, but not bumetanide-treated animals injected with midazolam (Mid; Fig. 7b).

Next, we assessed TrkB activation by Western blot with an antibody against phosphorylated TrkB (Y816) in bumetanide- and vehicle-treated pups after acute midazolam injection. In keeping with the RT-PCR data, we found that $GABA_A$-receptor activation enhanced TrkB phosphorylation in vehicle-, but not bumetanide-treated pups (Fig. 7c). Altogether, these results suggest that early interference with depolarizing GABA by bumetanide treatment impairs both synthesis and release of BDNF.

To investigate whether the perinatal decrease in BDNF signaling mediated the effects of early bumetanide treatment on visual cortical plasticity later in life, we performed a rescue experiment by increasing BDNF signaling concomitant to the bumetanide treatment. In particular, we injected bumetanide together with BDNF-mimetic drug 7,8-dihydroxyflavone

(DHF; i.p., 5 mg/Kg [28] from P3 to P8; Fig. 7d), which induces TrkB phosphorylation in the cortex *in vivo* [28]. Co-infusion of DHF and bumetanide during early development normalized the level of plasticity at P35 both *in vivo* (Fig. 7e,f) and *in vitro* (Fig. 7g,h). Interestingly, DHF treatment *per se* did not interfere with plasticity, as WM-LTP induction at P26 in rats treated perinatally with DHF or vehicle showed comparable levels of plasticity (Supplementary Fig. 10). Importantly, co-treatment of DHF together with bumetanide also rescued inhibitory GABAergic transmission (Fig. 8a), BDNF expression (Fig. 8b) and PNNs (Fig. 8c). Thus, disruption of the positive feedback regulation between depolarizing GABA and BDNF during early development accounts for the effects of early bumetanide treatment on the plasticity of the visual system later in life.

DISCUSSION

Also *Depolarizing* GABA controls CP plasticity

Hyperpolarizing and inhibitory GABA plays a major role in regulating CP plasticity in the visual cortex [5-7, 14]. In particular, opening of the CP needs reaching of a threshold level in the development of GABAergic inhibition [6], whereas complete development of GABAergic inhibition leads to the closure of the time window of maximal plasticity [5, 7]. Unlike in the adult, GABA depolarizes neuronal cells during early development, and it represents the main excitatory drive for immature cortical networks [8]. Consequently, depolarizing GABA is implicated in a series of developmental processes, including neuronal migration and morphological differentiation, as well as synapse maturation in the cortex [8-9]. For the first time here, we report a key role for early *depolarizing* GABA in the long-lasting control of the plasticity of neuronal circuits.

To interfere with early GABA action, we used systemic administration of the NKCC1-inhibitor bumetanide, with timing and doses effective in abolishing GABA-induced depolarization [10]. Plasticity of cortical circuits was evaluated by two independent measures, i.e., susceptibility to brief MD *in vivo* and induction of LTP in brain slices *in vitro*. Both approaches clearly indicated a protracted time window for plasticity in animals treated perinatally with bumetanide. Treatment with another NKCC1 inhibitor, furosemide, yielded a similar effect on CP plasticity at P35. Nevertheless, since changes in the volume of the extracellular fluid can potently impact on brain excitability [21], we tested whether the effects of NKCC1 inhibition were secondary to alterations of cell volume described upon diuretic treatment [20-22] rather than to regulation of Cl^- homeostasis. We found that early treatment with the osmotic diuretic mannitol –which does not regulate NKCC1 activity– failed to replicate the effect on plasticity. Altogether, our experimental evidence adds to the vast literature on the role of GABA in the control of visual cortical plasticity, indicating for the first time that not only hyperpolarizing but also *depolarizing* GABA plays an important role.

Early depolarizing GABA specifically controls plasticity

The decline of susceptibility to MD and WM-LTP induction temporally correlates with the development of visual functions, assessed in terms of maturation of visual acuity [1, 5]. In a number of studies, manipulations impacting the time course of the CP also affected the overall development of the visual system. For example, rearing animals in darkness

constrains the visual system in an immature state with decreased visual acuity, which is coupled to a prolongation of the window of susceptibility to MD and WM-LTP [15, 29]. Conversely, manipulations leading to precocious closure of the CP for plasticity such as environmental enrichment [3], administration of IGF1 [30], or BDNF overexpression [5, 29] also cause an accelerated cortical development (i.e., early maturation of visual acuity).

Thus, the physiological development and plasticity of the visual cortex have been classically considered as two strongly intermingled processes, with maturation of visual function being ineludibly linked to a waning of the potential for experience-dependent modifications [1]. Our results indicate in fact, that at least under certain conditions, the two processes may be regulated independently, as seen for other individual response properties in developing cortical networks [31-32]. Indeed, we found that early GABA interference prolonged the time window for plasticity, while leaving overall anatomical and physiological maturation of the visual system unaffected. We documented clear segregation of retino-geniculate fibers in the dLGN, no alteration in migration/morphological maturation of layer II/III pyramidal neurons and normal laminar distribution of interneurons in the visual cortex. Visual acuity, binocularity, contrast threshold, VEP amplitude and latency were within the normal range at P35, the same age at which consistent and significant plasticity could be induced only in bumetanide-treated animals.

The combined regulation of CP plasticity and overall visual system development found in previous studies (i.e., dark rearing from birth [15], BDNF overexpression in transgenic mice [5, 29], environmental enrichment from birth [3], or IGF-1 administration post-weaning [30]) , may depend on the fact that these long-lasting experimental protocols set in motion a number of different pathways acting in parallel to regulate physiological maturation and simultaneously delimit experience-dependent plasticity. Conversely, we found that an early and selective NKCC1 inhibition left a specific mark on developing cortical circuits, only impacting on the duration of the plasticity window.

At the functional level, the dissociation between CP plasticity and overall visual system development may be convenient, as cortical networks may remain customizable by experience even at the completion of the period of physiological maturation. This idea is consistent with the robust plasticity described in fully mature mice upon prolonged MD [14].

The absence of gross neuroanatomical defects in bumetanide-treated animals are seemingly in contrast with the reported alteration of cortical-neuron morphology upon treatment with bumetanide starting from embryonic stage to the first postnatal week [10]. This discrepancy may be due to a longer time period of the previous treatment (E15-P7) in comparison to our manipulation (P3-P8). Moreover, treatment from E15 to P7 includes time of delivery. As delivery is associated with a dramatic shift of GABA action from depolarizing to hyperpolarizing [33-34], part of the discrepancy with our results could depend on the fact that manipulation from E15 to P7 includes a time period in which GABA is not depolarizing.

Early depolarizing GABA and BDNF exert long-term control of CP regulators

Critical period plasticity in the visual cortex is controlled by fundamental regulators such as inhibitory GABAergic transmission, BDNF and the extracellular matrix [14]. In particular,

GABAergic inhibition and PNNs are considered as classical "plasticity brakes" [4] because their downregulation in adulthood effectively restores the sensitivity of cortical networks to MD and WM-LTP [7, 25, 35]. In keeping with this idea, the high plasticity of bumetanide-treated rats at P35 was accompanied by a decrease in inhibitory neurotransmission, in the number of PNNs and in BDNF levels. Importantly, we found that the GABA inhibitory tone was involved in the higher OD plasticity of bumetanide-treated rats at P35, as enhancing GABAergic transmission with diazepam significantly dampened the response to MD. Finally, we found no difference in the expression of these "brakes" at ages when plasticity was the same between bumetanide- and vehicle-treated animals (P26, peak of the CP; P75, adulthood). The amplitude and frequency of GABAergic events that we recorded at all ages are lower than in other studies utilizing access resistances lower than ours [36-39], although the frequency that we reported here is in agreement with a recent study utilizing an access resistance similar to ours[32].

Beside their coordinated effect on visual cortex plasticity, GABAergic transmission, BDNF and the extracellular matrix interact with one another also in the control of visual cortex development [5, 25, 40]. For example, activation of $GABA_A$ receptors by depolarizing GABA during early development triggers synthesis and release of BDNF [26-27]. The consequent activation of TrkB, in turn, promotes cell surface expression of $GABA_A$ receptors, leading to a positive feedback loop [26]. We found that disruption of this positive loop was a key event in the plasticizing effects of bumetanide treatment. Indeed, BDNF signaling downstream of $GABA_A$ receptor activation was significantly impaired in bumetanide-treated pups, and the long-term consequences of NKCC1 inhibition (i.e., increased plasticity at P35) were counteracted by TrkB activation *via* DHF treatment. Importantly, restoration of a normal closure of the CP by early DHF and bumetanide co-treatment was also accompanied by recovery of the normal levels of GABAergic inhibition, PNNs and BDNF, confirming the tight correlation between functional plasticity and these plasticity brakes. On the other hand, DHF treatment *per se* did not alter cortical plasticity. Altogether, these findings demonstrate that the loop between *depolarizing* GABA and BDNF during early development regulates the widely described interaction between *hyperpolarizing* GABA, BDNF and PNNs, major regulators of the CP plasticity later in life.

Mechanisms of CP regulation by early depolarizing GABA

Our data demonstrate that BDNF signaling is a crucial mediator of the effects of early depolarizing GABA on cortical inhibition and plasticity later in development. But what are the mechanisms that may account for the long-term, plasticizing effects of a transient interference with depolarizing GABA?

At least three different mechanisms (working alone or in combination) can be hypothesized. First, depolarizing GABA signaling might directly [41] or indirectly *via* BDNF [26-27] promote the subsequent maturation of inhibitory circuitry necessary for the closure of the CP [5, 7]. Nevertheless, this hypothesis seems unlikely. As GABAergic inhibition is also necessary for the opening of the CP, if the above hypothesis were true, one would expect a temporal shift of the whole CP rather than its mere prolongation, as found in the current study.

Second, spontaneous activity (prior to the onset of visual experience) and visually evoked discharges represent a continuum that acts to determine and instruct visual circuit development and plasticity [8, 42]. By definition, the CP is a phase of heightened sensitivity to environmental stimuli during which cortical networks are customized by visual experience [14]. When network activity is reduced, such as in dark rearing, the visual system reacts with an extension of the CP to prolong the effective time window during which visual experience can instruct circuit refinement [15]. In this context, a precocious reduction of GABA-mediated excitation during early development may trigger extended plasticity of the visual cortex as a way to compensate for the early loss of wiring instructions coded by the spontaneous activity patterns. The specific effect of early bumetanide treatment on the closure (and not the opening) of the CP, together with the retention of a juvenile-like plasticity at P35 would favor this hypothesis.

A third possible explanation for the long-term effects of early GABA interference resides in epigenetic mechanisms [43-44] . Classic experiments showed that early environmental experiences (such as levels of early maternal care) influence adult behavior by modifications of chromatin structure [45]. Thus, we speculate that a transient interference with GABA-mediated excitation may leave persistent marks on specific classes of cortical neurons, reverberating on altered function and structure (i.e., reduced inhibitory transmission and reduced PNN) later in life. These epigenetic changes could display their effects at specific developmental stages (i.e., P35) with no apparent impact on the initial, “default” developmental trajectory of plasticity and its regulators.

Therapeutic perspective

Bumetanide is a FDA-approved drug extensively used in the past as a loop diuretic and currently used to treat heart failure and respiratory disorders in infancy [20]. Interestingly, due to its ability to inhibit the brain-specific transporter NKCC1, bumetanide has been proposed as a promising candidate to treat brain diseases [46], based on studies in animal models [12, 34, 46] and recent clinical trials [46-48]. However, the use of this drug in neonates has been partially questioned [10, 49-50] due to the key role played by depolarizing GABA during early development [8]. Our data similarly suggest possible *long-term* consequences of NKCC1 inhibition during early development. On the other hand, our study also sheds light on the existence of therapeutic windows for pharmacological interventions aimed at prolonging CP plasticity, without affecting overall neuronal circuit development [46].

METHODS

Animal treatment

All procedures were approved by IIT licensing, the Italian Ministry of Health and EU guidelines (Directive 2010/63/EU). Long Evans rats were housed at 21°C, 12 h light/dark cycle, and food/water *ad libitum*. Female and male littermates were injected i.p. twice a day, from P3 to P8, with bumetanide (0.2 mg/Kg, SIGMA), furosemide (20 mg/Kg, SIGMA), DHF (5 mg /Kg, SIGMA) or vehicle (DMSO, 0.04% in physiological solution) and once a day with mannitol (7.5 g/Kg, SIGMA). For midazolam experiments, vehicle and bumetanide-treated pups received one injection at P8 (i.p., 5 mg/Kg, IBI). MD was

performed as described [19]. A subset of rats treated perinatally with bumetanide were monocularly deprived at P35 and treated daily with diazepam (2 mg/Kg, i.p.[24]; kindly provided by Roche) to enhance $GABA_A$ergic inhibition, starting 4 hrs before eyelid suture. Rat body weights were monitored twice a day.

In vivo electrophysiology

Rats were anesthetized with Hypnorm/Hypnovel (in water; 0.375 mL/Kg; VetaPharma, UK) and the skull overlying the binocular visual cortex was drilled on one side. A glass micropipette (2 MΩ) filled with NaCl (3 M) was mounted on a motorized micromanipulator and inserted into the binocular visual cortex. Visual evoked potentials (VEPs) were recorded from 3–4 penetrations/animal and the electrode was positioned at 100 and 400 μm depth within the cortex. Electrical signals were amplified (10,000 fold), band-pass filtered (0.3 – 100 Hz), digitized and averaged in synchrony with the stimulus contrast reversal. Analysis of the amplitude of VEP responses was performed blind to animal treatment. Visual stimuli were gratings of various spatial frequencies and contrast generated by a VSG2/5 card (Cambridge Research Systems, Rochester, UK) on a display (Sony Multiscan G500; mean luminance, 15 cd/m^2) positioned 20–30 cm from the rat's eyes to include the central visual field (110 × 85° of visual angle).

Steady-state VEPs: visual acuity and contrast threshold—VEP recordings in steady-state mode were used to measure spatial resolution and contrast threshold. The visual response was measured as the amplitude (μV) of the second harmonic of the stimulation frequency (4 Hz), calculated after Fourier analysis of the signal. Visual acuity was assessed after presentation of gratings of variable spatial frequencies (90% contrast). Visual acuity was determined by extrapolation to 0 V of the linear regression through the 4–6 points closest to noise level in a curve where VEP amplitude was plotted against log spatial frequency. In the same temporal frequency (4 Hz), we analyzed contrast threshold in response to 0.07 cycles per degree (c/deg) gratings. Contrast threshold was taken as the lowest contrast that evoked a VEP response greater than the mean value of the noise.

Transient VEPs: C/I ratio and degree of plasticity—Transient VEPs were recorded in response to the abrupt contrast reversal (1 Hz) of a square-wave grating (spatial frequency 0.1 c/deg, contrast 90%). For each animal, we calculated a C/I ratio, i.e., the ratio of VEP amplitudes recorded by stimulating the contralateral and ipsilateral eye. We summarized the level of OD plasticity *in vivo* for each age/treatment by calculating an index (degree of plasticity). The average value of this quantity, i.e. mean (index), was obtained by subtracting the mean value of the C/I ratio of the MD group – mean ($[C/I]_{MD}$) – from that of the nonMD animals – mean ($[C/I]_{nonMD}$) – of the same age/treatment:

$$\text{mean (index)} = \text{mean}\left([C/I]_{nonMD}\right) - \text{mean}\left([C/I]_{MD}\right)$$

The variance –var– of this index incorporates the uncertainties of both nonMD and MD groups, according to the error propagation formula:

$$\mathrm{var}\,(\mathrm{index}) = \mathrm{var}\left([\,C/I]_{nonMD}\right) + \mathrm{var}\left([\,C/I]_{MD}\right)$$

In vitro electrophysiology

For acute visual cortex slices, rats were anesthetized with isoflurane and transcardially perfused with an ice-cold cutting solution with the following composition (in mM): 0.1 $MgCl_2$; 2.5 KCl; 1.25 NaH_2PO_4; 2 $MgSO_4$; 0.1 $CaCl_2$; 26 $NaHCO_3$; 206 Sucrose and 12 D-Glucose (~300 mOsm, pH 7.4, oxygenated with 95 % O_2 and 5 % CO_2). Coronal slices (350 μm thick; VT1000S, Leica Microsystems vibratome) were incubated at 35°C for 30 min in artificial cerebrospinal fluid (ACSF) with the following composition (in mM): 124 NaCl; 2.5 KCl; 1.25 NaH_2PO_4; 2 $MgSO_4$; 2 $CaCl_2$; 26 $NaHCO_3$; 0.02 sulfinpyrazone; 1 ascorbic acid; 0.5 myo-inositol; 2 pyruvic acid and 12 D-Glucose (~310 mOsm, pH 7.4), oxygenated with 95 % O_2 and 5 % CO_2. After 1 h recovery at RT, slices were perfused with ACSF (35°C, 1.7 mL/min).

WM-LTP recordings—Electrical stimulation (100 μs duration) was delivered by a bipolar concentric stimulating electrode (FHC, St. Bowdoinham, ME) placed at the border of the WM and layer VI. Field potentials in layer II/III of the binocular visual cortex were recorded by a micropipette (1–3 MΩ) filled with NaCl (3 M). Baseline responses were obtained every 30 s with a stimulation intensity that yielded a half-maximal response. After 10 min of stable baseline, a theta-burst stimulation (TBS) was delivered. The protocol of TBS stimulation consisted of 2 trains of TBS every 10 s. Each TBS train consisted of 12 bursts at 5 Hz. Each burst consisted of 4 pulses at 100 Hz. Data, filtered at 0.1 Hz and 3 kHz and sampled at 25 kHz were acquired with a patch-clamp amplifier (Multiclamp 700, Molecular Devices), and analyzed using pClamp 10.2 software (Molecular Devices).

Patch-clamp recordings—Whole-cell patch-clamp recordings were made from layer II/III pyramidal neurons of the binocular visual cortex at RT. Glass micropipettes (resistance, 4–8 MΩ) were filled with an internal solution of (in mM): 120 K^+ Gluconate; 20 KCl; 10 HEPES; 0.1 EGTA; 2 $MgCl_2$; 10 phosphocreatine Na_2^+; 2 Mg^{2+}ATP; 0.25 Na_2GTP (~300 mOsm, pH 7.4). The membrane resting potential was measured immediately after whole-cell access at 0 current. Criteria for accepting a recording included an input resistance > 200 MΩ and a access resistance < 25 MΩ, with a maximal variation of 20%. Capacitance, input, and access resistance were measured online with Clampex 10.2. For mPSCs, the holding potential was set at –70 mV and gap-free recordings were performed for 5 minutes in tetrodotoxin (TTX, 0.2 μM, Tocris) to establish the baseline of mPSC frequency. Then, DNQX (20 μM, Tocris) was bath applied for 5 min to isolate inhibitory mPSCs (mIPSCs). Application of both bicuculline methiodide (25 μM, Sigma) and DNQX abolished all mPSCs. mEPSCs frequency was calculated by subtracting the frequency of mIPSCs from the frequency of baseline mPSC. Data, filtered at 0.1Hz and 5 kHz, and sampled at 25 kHz were acquired with a patch-clamp Multiclamp 700 amplifier, and analyzed using pClamp 10.2 software. All chemicals were purchased from Sigma, unless otherwise specified.

Europe PMC Funders Author Manuscripts

Labeling and analysis of retino-geniculate axons

Labeling of retino-geniculate axons was performed as previously [18, 51]. Rats received an intravitreal injection of Cholera Toxin B subunit (CTB) conjugated with Alexa Fluor 488 (10 mg/mL, Invitrogen) into the left eye and CTB-Alexa Fluor 594 (10 mg/mL, Invitrogen) into the right eye two days before perfusion. Animals were perfused transcardially with 4% paraformaldehyde (PFA) in 0.1 M phosphate buffer. Brains coronal sections were cut on a freezing microtome (50 μm thick), and collected in a serial order through the entire thalamus.

CTB labels were examined with a Leica Confocal microscope using a 10X objective (air, NA 0.4). For each animal, we acquired the five largest sections through the middle of the dLGN [18]. The relative areas occupied by the ipsilateral and contralateral projections were calculated by dividing the average of the five ipsilateral or contralateral areas by the average of the five total dLGN areas. To determine the extent of overlap between ipsilateral and contralateral projections to the same dLGN, the ipsilateral and contralateral areas were measured, and their sum was subtracted from the total dLGN area and expressed as a percentage of it.

Tripolar *in utero* electroporation of the visual cortex

Tripolar *in utero* electroporation of the visual cortex was performed as previously [52]. Timed-pregnant Long Evans rats were anaesthetized at E17.5 with isoflurane (induction, 3.5%; surgery, 2.5%), and uterine horns were exposed by laparotomy. Expression vectors (pCAG-IRES-EGFP, 1.5 μg/μL in water) and dye Fast Green (0.3 μg/μL; Sigma, St. Louis, MO) were injected (5–6 μL) through the uterine wall into one of the embryos' lateral ventricles by a 30-G needle. While the embryo's head was carefully held between standard forceps-type circular electrodes (10 mm diameter; positive poles; Nepa Gene, Chiba, Japan), a third electrode (7×6×1 mm, negative pole) was positioned on the back of the embryo's head. 5 electrical pulses (amplitude, 50V; duration, 50 ms; intervals, 100 ms) were delivered with a square-wave electroporation generator (CUY21EDIT; Nepa Gene). Uterine horns were returned into the abdominal cavity, and embryos continued their normal development.

Slice histology—P35 rats were transcardially perfused with 4% PFA in 0.1 M PB, pH 7.4. Brains were cut coronally (80 μm thick) with a freezing microtome. Free-floating slices were permeabilized and blocked with PBS containing 0.3% Triton X-100, 10% normal goat serum (NGS, Jackson ImmunoResearch), 0.2% BSA and then incubated with anti-NeuN antibody (mouse anti-NeuN, 1:1000, Sigma) followed by Alexa-568 fluorescent secondary antibody (1:600, Invitrogen).

Confocal image acquisition and analysis—For high-magnification images of cell morphology of EGFP-transfected neurons, 80 μm-thick z-stacks were acquired with a 20X objective (oil, 0.7 NA), and Z-series were projected to two-dimensional representations followed by neurite tracing and quantification with the NeuronJ plugin of ImageJ software.

Immunohistochemistry

Animals were deeply anesthetized and perfused with 4% PFA in 0.1 M PB, pH 7.4. Brains were cut coronally with a freezing microtome. For PV immunostaining, free-floating sections were blocked for 2 h at RT with 10% NGS, 0.3% Triton X-100 in PBS. Slices were incubated overnight at 4°C with anti-parvalbumin primary antibody (guinea pig polyclonal, #195004, 1:1,000, Synaptic Systems, [53]), followed by donkey anti-guinea pig DyLight-488 (1:200, Jackson Immuno Research). For PNNs labelling, we used the lectin Wisteria floribunda agglutinin (WFA, #L1516-2mg) [25]. The blocking solution contained 3% BSA in PBS, and biotinylated WFA (1% BSA in PBS, 1:100, Sigma) was applied overnight at 4°C. WFA was revealed with 1 h incubation in Cy3-conjugated ExtrAvidin (1:500, Sigma). For GAD67 immunostaining, the blocking solution contained 10% NGS, 3% BSA, 0.3% Triton X-100 in PBS. Anti-GAD67 (mouse monoclonal, #MAB5406, 1:500, Millipore, [54]) was applied overnight at 4°C. Signal was revealed with 1 h incubation in biotin-conjugated secondary antibody and streptavidin-conjugated fluorophore (Alexa 594, 1:500, Life Technologies).

For immunohistochemistry quantifications, PNNs and PV cells were counted blind to treatment on a fluorescence microscope using a 40X objective (oil, 1.25 NA) and StereoInvestigator software (Microbrightfield). Cells were counted in vertical columns (250 μm width) spanning the entire thickness of primary visual cortex. 6–8 sections were analyzed for each experimental animal. For colocalization analysis, we calculated the percentage of PV-positive cells surrounded by PNNs. Count of GAD67 cells was performed on 3 sections for each experimental animal. For each section, images of the visual cortex were acquired with a 20X objective (air, 0.5 NA) by a Zeiss AxioObserver z1 microscope with a motorized stage. Acquisitions were automatically performed using the MosaiX and Z-Stack modules of the Zeiss AxioVision software (v4.3.1). Five Z-series for each image were projected to two-dimensional representations. Cells were separately counted in layers II–III, IV, V–VI of the primary visual cortex with the Adobe Photoshop software (200 × 600 μm counting frame). Only cells larger than 5 μm with a clearly visible nucleus were counted. For the counting of PV-boutons, confocal images from layers II/III of the visual cortex were acquired with a 60X objective (oil, 1.4 NA) using a confocal microscope (A1, Nikon). Two fields for each animal were analyzed. Perisomatic PV-boutons around putative cell somas were counted using a NIS-Elements AR software, and expressed as number of boutons per cell soma in a single (largest) focal section, as previously described [55]. For each animal, bouton densities from at least 15 cell somas were averaged. For all experiments, data acquisition and quantification was performed blind to the treatment.

Eye-opening observations

From P11, rat pups were inspected for eye opening twice daily. Eye opening was defined as the initial break in the membrane sealing the lids of both eyes.

Prusky water maze

Rats were tested blind to treatment in the visual water task, as previously [3, 19]. The apparatus consisted of a trapezoidal-shaped pool, filled with opaque water, partially divided at one end in two arms by a divider. Visual stimuli consisted of gratings or gray fields, generated with

two computer monitors and placed at the end of each arm. A hidden platform was placed below the grating. During the learning phase (P17/19 to P23/24), visual stimuli consisted of gratings of low spatial frequency (0.1 cycles/degree). Animals were trained to associate the stimulus grating with the submerged platform. We reported the performance in learning the task as the % of correct choices over the training sessions.

Behavioural assessment of visual acuity was performed from P24 to P32. The limit of the discrimination was estimated by increasing the spatial frequency of the grating until performance fell below 70% accuracy. For each rat, distinct sessions of visual acuity estimate were run three times a day every other day. A frequency of seeing curve was constructed from the total data, and the spatial frequency corresponding to 70% accuracy was taken as the acuity value [19].

Serum collection and osmolarity measurement

Ten minutes after a single bumetanide i.p. injection at P8, rat pups were deeply anesthetized and blood collection was performed by cardiac puncture. Samples were centrifuged (Centrifuge 5417R, Eppendorf) and osmolarity of recovered serum was estimated by a Vapor pressure osmometer (Wescor).

Western blot

Western blot experiments were performed as previously [3, 19]. Rats were deeply anesthetized and the primary visual cortex was dissected out. Proteins were extracted with lysis buffer (1% Triton X-100, 10% glycerol, 20 mM Tris-HCl, pH 7.5, 150 mM NaCl, 10 mM EDTA, 0.1 mM Na_3VO_4, 1 μg/mL leupeptin, 1 μg/mL aprotinin, and 1 mM PMSF). Protein extracts (10–50 μg per lane, depending on the protein) were boiled for 5 min at 100 °C, loaded on Bis-Tris 4–12% precast gels (Bio-Rad), separated using SDS-PAGE (1 h at 200 V), and blotted on nitrocellulose membrane (Bio-Rad). Blots were blocked using a solution of 4% milk and 0.2% Tween-20 in Tris-buffered solution (TBS) for 2 h at RT. The primary antibodies anti-NKCC1 (mouse monoclonal, #T4, 1:500, DSHB, [56]), anti-KCC2 (rabbit polyclonal, #07-432, 1:1000, Millipore, [56]), anti-BDNF (rabbit polyclonal, # sc-546, 1:200, Santa Cruz), anti-p-TrkB (rabbit, 1:1000, kindly provided by Dr. Moses V. Chao), anti-TrkB (mouse monoclonal, #610101, 1:1000, BD Biosciences, [57]) were applied overnight at 4°C in blocking solution containing 2% milk and 0.1% Tween-20 in TBS. Blots were then incubated with 1:20,000 horseradish peroxidase (HRP)-conjugated anti-secondary antibodies (Jackson Immunoresearch, West Grove, PA) for 2 h at RT to reveal the signal in chemiluminescence (ECL) using the luminol/enhancer system (Immun-Star Western C; Bio-Rad) and autoradiography films (HyperFilm; GE Healthcare). In selected experiments, we used secondary antibodies conjugated with infrared-emitting dyes (rabbit IRDye® 800CW, 1:20,000 or mouse IRDye® 680RD, 1:20,000, Li-Cor Biosciences; incubated for 1 h at RT) and revealed the signal with the Odyssey scanner system (Li-Cor Biosciences). Films or filters were scanned using an Epson scanner (Epson) or Odyssey IR scanner (Li-Cor), respectively. Densitometry analysis was performed with either ImageJ or Image Studio software version 3.1 (Li-Cor), respectively. As an internal standard, all blots were probed for α-tubulin (mouse monoclonal, 1:20,000, Sigma). For p-TkB signal, total TrkB expression was used for standardization.

Quantitative RT-PCR

Visual cortices were dissected 3h after midazolam treatment in P8 rat pups. Quantitative RTPCR was performed as previously [54]. Total RNAs were extracted (Trizol© reagent, Invitrogen), treated with DNAse, and purified with RNeasy Mini Kit (Qiagen, USA). cDNA was synthesized from RNAs (2 μg) using the SuperScript® VILO™ (Invitrogen Life Technologies, USA). Quantitative real-time PCR was performed using a CFX 384 thermal cycler with real-time detection of fluorescence (Biorad). Individual PCR reactions were conducted using the MESA GREEN qPCR kit (Eurogentec SA, Belgium). Primers (Sigma) were designed on different exons to avoid amplification of genomic DNA. Glyceraldehyde 3-phosphate dehydrogenase (Gapdh) was used as a standard for quantification. Primer sequences were as follows: *Bdnf Exon9a*, forward ATGGGCCACATGCTGTCCCCG, reverse TTCTGGTCCTCATCCAGCAGC; GAPDH, forward ACTAACCGTTGTCCCAATCT, reverse CTCTTGCTCTCAGTATCCTT. Each PCR cycle consisted of denaturation for 10 s at 94 °C, annealing for 20 s at 60 °C and extension for 30 s at 72 °C. The fluorescence intensity of SYBR green was read and acquired at 72 °C after completion of the extension step of each cycle. PCR conditions for individual primer sets were optimized by varying template cDNA and primer concentration in order to obtain a single PCR product and amplification efficiency > 90% [54]. Relative expression values were calculated using DCt method. Mean cycle threshold values from triplicate experiments (Ct) were calculated for *Bdnf Exon 9a* and *Gapdh*, and corrected for PCR efficiency and inter-run calibration. Bdnf / Gapdh ratios were then calculated for each sample.

Statistical analysis

Statistical analysis was performed with SigmaPlot 11.0. Sample size was calculated by the sample-size calculator in Sigma-plot 11.0 (power > 0.05; alpha = 0.05). All data were run for a normality test by default in SigmaPlot 11.0 before any statistical comparison test. Data normally distributed were summarized by mean ± SEM, whereas data non-normally distributed were summarized with percentiles and a box chart. Pairwise comparisons of quantitative phenotypes between rats of different groups were assessed by a two-tailed Student's *t*-test. When more than two groups/factors were analyzed, one/two-way ANOVA followed by Holm-Sidak/Tukey/Duncan test or one-way ANOVA on ranks with Dunn's *post hoc* test were used for data normally or not normally distributed, respectively. For the analysis of learning in the Prusky water box and the longitudinal measurement of behavioural visual acuity, we run a two way repeated measures ANOVA. Eye opening observations were compared with a χ^2 test. A Grubbs' test (extreme studentized deviate) was performed to verify for the presence of outliers in the data sets. Level of significance was $P < 0.05$.

Method for sample randomization: For image acquisition at the confocal microscope, all slides were acquired in a random order and in a single session for each litter of animals to minimize errors caused by fluctuation in laser output and degradation of fluorescence. For electrophysiological recordings, care was used to record from one bumetanide- and one vehicle-injected animal on alternating days. For LTP, MD and behavioral experiments, animals treated with bumetanide or vehicle were litter mates.

Where not otherwise specified, data collection and analysis were not performed blind to the conditions of the experiments.

Supplementary Material

Refer to Web version on PubMed Central for supplementary material.

ACKNOWLEDGEMENTS

We thank Dr. K. Kaila (University of Helsinki, Finland) for providing brain tissue from NKCC1 knock out brains for control experiments. We thank Dr. Maria Cristina Cenni (CNR, Pisa, Italy) for providing the protocol for retino-geniculate axons labelling. We thank Dr. Moses V. Chao (New York University School of Medicine, New York, USA) for kindly providing anti-p-TrkB. We thank Dr. F. Benfenati (IIT, Genoa, Italy) for reading the manuscript. The work was supported by Compagnia di San Paolo (grant # 2008.1267 to LC and MC), Telethon (grants # GGP10135 to LC, GGP11116 to MC, GGP13187 to LC), Italian Ministry of Research (PRIN 2010-2011 grant # 2010N8PBAA_002 to Y.B.), University of Trento (CIBIO start-up grant to Y.B.).

REFERENCES

1. Berardi N, Pizzorusso T, Maffei L. Critical periods during sensory development. Curr Opin Neurobiol. 2000; 10:138–145. [PubMed: 10679428]
2. Espinosa JS, Stryker MP. Development and plasticity of the primary visual cortex. Neuron. 2012; 75:230–249. [PubMed: 22841309]
3. Cancedda L, et al. Acceleration of visual system development by environmental enrichment. J Neurosci. 2004; 24:4840–4848. [PubMed: 15152044]
4. Morishita H, Hensch TK. Critical period revisited: impact on vision. Curr Opin Neurobiol. 2008; 18:101–107. [PubMed: 18534841]
5. Huang ZJ, et al. BDNF regulates the maturation of inhibition and the critical period of plasticity in mouse visual cortex. Cell. 1999; 98:739–755. [PubMed: 10499792]
6. Fagiolini M, Hensch TK. Inhibitory threshold for critical-period activation in primary visual cortex. Nature. 2000; 404:183–186. [PubMed: 10724170]
7. Harauzov A, et al. Reducing intracortical inhibition in the adult visual cortex promotes ocular dominance plasticity. J Neurosci. 2010; 30:361–371. [PubMed: 20053917]
8. Ben-Ari Y, et al. Refuting the challenges of the developmental shift of polarity of GABA actions: GABA more exciting than ever! Front Cell Neurosci. 2012; 6:35. [PubMed: 22973192]
9. Sernagor E, Chabrol F, Bony G, Cancedda L. GABAergic control of neurite outgrowth and remodeling during development and adult neurogenesis: general rules and differences in diverse systems. Front Cell Neurosci. 2010; 4:11. [PubMed: 20428495]
10. Wang DD, Kriegstein AR. Blocking early GABA depolarization with bumetanide results in permanent alterations in cortical circuits and sensorimotor gating deficits. Cereb Cortex. 2011; 21:574–587. [PubMed: 20624842]
11. Cleary RT, et al. Bumetanide enhances phenobarbital efficacy in a rat model of hypoxic neonatal seizures. PLoS One. 2013; 8:e57148. [PubMed: 23536761]
12. Dzhala VI, et al. NKCC1 transporter facilitates seizures in the developing brain. Nat Med. 2005; 11:1205–1213. [PubMed: 16227993]
13. Sipila ST, Schuchmann S, Voipio J, Yamada J, Kaila K. The cation-chloride cotransporter NKCC1 promotes sharp waves in the neonatal rat hippocampus. J Physiol. 2006; 573:765–773. [PubMed: 16644806]
14. Levelt CN, Hubener M. Critical-period plasticity in the visual cortex. Annu Rev Neurosci. 2012; 35:309–330. [PubMed: 22462544]
15. Fagiolini M, Pizzorusso T, Berardi N, Domenici L, Maffei L. Functional postnatal development of the rat primary visual cortex and the role of visual experience: dark rearing and monocular deprivation. Vision Res. 1994; 34:709–720. [PubMed: 8160387]

Europe PMC Funders Author Manuscripts

16. Frenkel MY, Bear MF. How monocular deprivation shifts ocular dominance in visual cortex of young mice. Neuron. 2004; 44:917–923. [PubMed: 15603735]
17. Cancedda L, Fiumelli H, Chen K, Poo MM. Excitatory GABA action is essential for morphological maturation of cortical neurons in vivo. J Neurosci. 2007; 27:5224–5235. [PubMed: 17494709]
18. Menna E, Cenni MC, Naska S, Maffei L. The anterogradely transported BDNF promotes retinal axon remodeling during eye specific segregation within the LGN. Mol Cell Neurosci. 2003; 24:972–983. [PubMed: 14697662]
19. Caleo M, et al. Transient synaptic silencing of developing striate cortex has persistent effects on visual function and plasticity. J Neurosci. 2007; 27:4530–4540. [PubMed: 17460066]
20. Maa EH, Kahle KT, Walcott BP, Spitz MC, Staley KJ. Diuretics and epilepsy: will the past and present meet? Epilepsia. 2011; 52:1559–1569. [PubMed: 21838793]
21. Hochman DW. The extracellular space and epileptic activity in the adult brain: explaining the antiepileptic effects of furosemide and bumetanide. Epilepsia. 2012; 53(Suppl 1):18–25. [PubMed: 22612805]
22. Haglund MM, Hochman DW. Furosemide and mannitol suppression of epileptic activity in the human brain. J Neurophysiol. 2005; 94:907–918. [PubMed: 15728766]
23. Hensch TK, et al. Local GABA circuit control of experience-dependent plasticity in developing visual cortex. Science. 1998; 282:1504–1508. [PubMed: 9822384]
24. Greifzu F, et al. Environmental enrichment extends ocular dominance plasticity into adulthood and protects from stroke-induced impairments of plasticity. Proc Natl Acad Sci U S A. 2014; 111:1150–1155. [PubMed: 24395770]
25. Pizzorusso T, et al. Reactivation of ocular dominance plasticity in the adult visual cortex. Science. 2002; 298:1248–1251. [PubMed: 12424383]
26. Porcher C, et al. Positive feedback regulation between gamma-aminobutyric acid type A (GABA(A)) receptor signaling and brain-derived neurotrophic factor (BDNF) release in developing neurons. J Biol Chem. 2011; 286:21667–21677. [PubMed: 21474450]
27. Mantelas A, Stamatakis A, Kazanis I, Philippidis H, Stylianopoulou F. Control of neuronal nitric oxide synthase and brain-derived neurotrophic factor levels by GABA-A receptors in the developing rat cortex. Brain Res Dev Brain Res. 2003; 145:185–195. [PubMed: 14604759]
28. Jang SW, et al. A selective TrkB agonist with potent neurotrophic activities by 7,8-dihydroxyflavone. Proc Natl Acad Sci U S A. 2010; 107:2687–2692. [PubMed: 20133810]
29. Gianfranceschi L, et al. Visual cortex is rescued from the effects of dark rearing by overexpression of BDNF. Proc Natl Acad Sci U S A. 2003; 100:12486–12491. [PubMed: 14514885]
30. Ciucci F, et al. Insulin-like growth factor 1 (IGF-1) mediates the effects of enriched environment (EE) on visual cortical development. PLoS One. 2007; 2:e475. [PubMed: 17534425]
31. Fagiolini M, et al. Separable features of visual cortical plasticity revealed by N-methyl-D-aspartate receptor 2A signaling. Proc Natl Acad Sci U S A. 2003; 100:2854–2859. [PubMed: 12591944]
32. Stephany CE, et al. Plasticity of binocularity and visual acuity are differentially limited by nogo receptor. J Neurosci. 2014; 34:11631–11640. [PubMed: 25164659]
33. Tyzio R, et al. Maternal oxytocin triggers a transient inhibitory switch in GABA signaling in the fetal brain during delivery. Science. 2006; 314:1788–1792. [PubMed: 17170309]
34. Tyzio R, et al. Oxytocin-mediated GABA inhibition during delivery attenuates autism pathogenesis in rodent offspring. Science. 2014; 343:675–679. [PubMed: 24503856]
35. Sale A, et al. Environmental enrichment in adulthood promotes amblyopia recovery through a reduction of intracortical inhibition. Nat Neurosci. 2007; 10:679–681. [PubMed: 17468749]
36. Gao M, et al. Rebound potentiation of inhibition in juvenile visual cortex requires vision-induced BDNF expression. J Neurosci. 2014; 34:10770–10779. [PubMed: 25100608]
37. Abidin I, Eysel UT, Lessmann V, Mittmann T. Impaired GABAergic inhibition in the visual cortex of brain-derived neurotrophic factor heterozygous knockout mice. J Physiol. 2008; 586:1885–1901. [PubMed: 18238806]
38. Jang HJ, et al. Layer-specific serotonergic facilitation of IPSC in layer 2/3 pyramidal neurons of the visual cortex. J Neurophysiol. 2012; 107:407–416. [PubMed: 22013240]

39. Maffei A, Lambo ME, Turrigiano GG. Critical period for inhibitory plasticity in rodent binocular V1. J Neurosci. 2010; 30:3304–3309. [PubMed: 20203190]
40. Beurdeley M, et al. Otx2 binding to perineuronal nets persistently regulates plasticity in the mature visual cortex. J Neurosci. 2012; 32:9429–9437. [PubMed: 22764251]
41. Chattopadhyaya B, et al. GAD67-mediated GABA synthesis and signaling regulate inhibitory synaptic innervation in the visual cortex. Neuron. 2007; 54:889–903. [PubMed: 17582330]
42. Huberman AD, Feller MB, Chapman B. Mechanisms underlying development of visual maps and receptive fields. Annu Rev Neurosci. 2008; 31:479–509. [PubMed: 18558864]
43. Mellios N, et al. miR-132, an experience-dependent microRNA, is essential for visual cortex plasticity. Nat Neurosci. 2011; 14:1240–1242. [PubMed: 21892155]
44. Tognini P, Putignano E, Coatti A, Pizzorusso T. Experience-dependent expression of miR-132 regulates ocular dominance plasticity. Nat Neurosci. 2011; 14:1237–1239. [PubMed: 21892154]
45. Weaver IC, et al. Epigenetic programming by maternal behavior. Nat Neurosci. 2004; 7:847–854. [PubMed: 15220929]
46. Deidda G, Bozarth IF, Cancedda L. Modulation of GABAergic transmission in development and neurodevelopmental disorders: investigating physiology and pathology to gain therapeutic perspectives. Front.Cell.Neurosci. 2014; 8
47. Lemonnier E, et al. A randomised controlled trial of bumetanide in the treatment of autism in children. Transl Psychiatry. 2012; 2:e202. [PubMed: 23233021]
48. Kahle KT, Barnett SM, Sassower KC, Staley KJ. Decreased seizure activity in a human neonate treated with bumetanide, an inhibitor of the Na(+)-K(+)-2Cl(−) cotransporter NKCC1. J Child Neurol. 2009; 24:572–576. [PubMed: 19406757]
49. Vanhatalo S, Hellstrom-Westas L, De Vries LS. Bumetanide for neonatal seizures: Based on evidence or enthusiasm? Epilepsia. 2009; 50:1292–1293. [PubMed: 19496810]
50. Chabwine JN, Vanden Eijnden S. A claim for caution in the use of promising bumetanide to treat neonatal seizures. J Child Neurol. 2011; 26:657–658. author reply 658-659. [PubMed: 21531912]
51. Allegra M, et al. Altered GABAergic markers, increased binocularity and reduced plasticity in the visual cortex of Engrailed-2 knockout mice. Front Cell Neurosci. 2014; 8:163. [PubMed: 24987331]
52. dal Maschio M, et al. High-performance and site-directed in utero electroporation by a triple-electrode probe. Nat Commun. 2012; 3:960. [PubMed: 22805567]
53. Antonucci F, et al. Cracking down on inhibition: selective removal of GABAergic interneurons from hippocampal networks. J Neurosci. 2012; 32:1989–2001. [PubMed: 22323713]
54. Sgado P, et al. Loss of GABAergic neurons in the hippocampus and cerebral cortex of Engrailed-2 null mutant mice: Implications for autism spectrum disorders. Exp Neurol. 2013; 247:496–505. [PubMed: 23360806]
55. Chattopadhyaya B, et al. Experience and activity-dependent maturation of perisomatic GABAergic innervation in primary visual cortex during a postnatal critical period. J Neurosci. 2004; 24:9598–9611. [PubMed: 15509747]
56. Ge S, et al. GABA regulates synaptic integration of newly generated neurons in the adult brain. Nature. 2006; 439:589–593. [PubMed: 16341203]
57. Jovanovic JN, Czernik AJ, Fienberg AA, Greengard P, Sihra TS. Synapsins as mediators of BDNF-enhanced neurotransmitter release. Nat Neurosci. 2000; 3:323–329. [PubMed: 10725920]

Europe PMC Funders Author Manuscripts

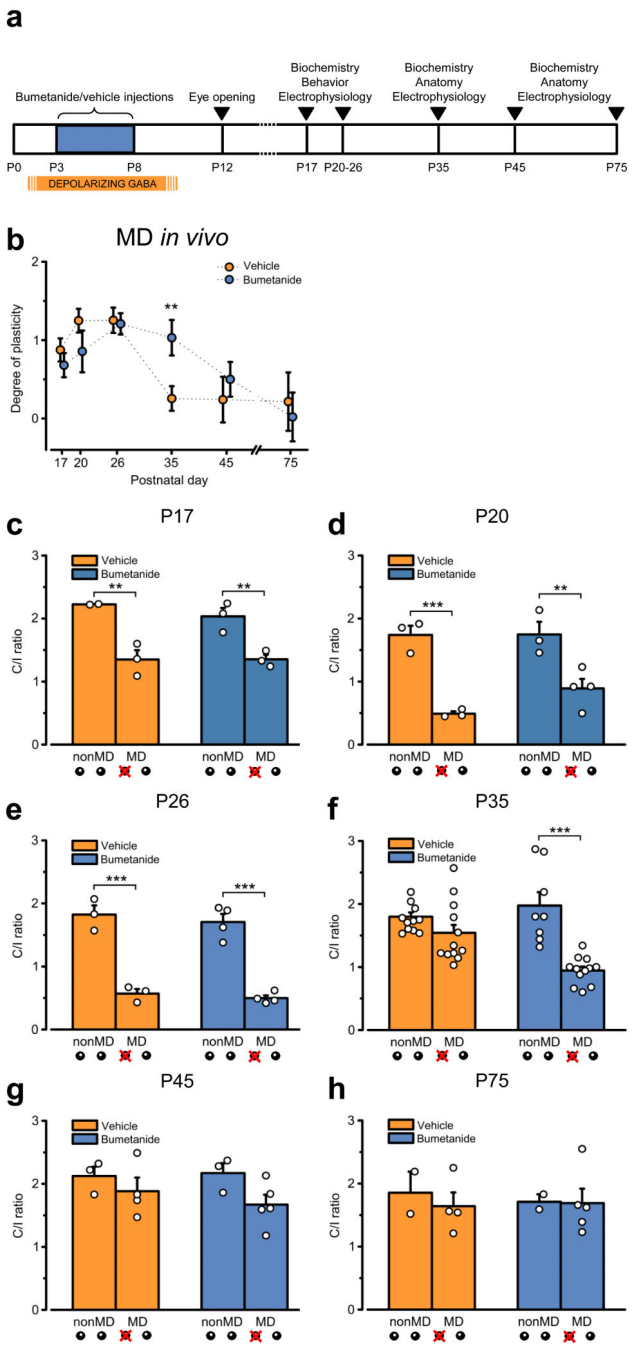

Figure 1.

Early GABAergic interference prolongs critical period plasticity in the visual cortex *in vivo*. (**a**) Schematic cartoon of the experimental protocol. (**b**) Average level of plasticity (quantified as described in the Methods section) ± standard error of the mean (SEM) derived from experiments performed at different ages and shown in panels (c–h). The level of plasticity was higher in bumetanide-treated animals (blue) than in vehicle controls (orange) at P35 (post Two Way ANOVA Holm-Sidak test, $P = 0.009$), but similar at P17, P20, P26, P45 and P75 ($P = 0.998, 0.916, 0.999, 0.988, 0.999$). (**c–h**) C/I VEP ratios measured at the

indicated ages in vehicle- (orange) or bumetanide-treated animals (blue), either non-deprived (nonMD) or monocularly deprived (MD). At all ages, baseline binocularity was super-imposable between bumetanide- and vehicle-treated rats (post Two Way ANOVA Tukey test; c: $P = 0.322$, d: $P = 0.972$, e: $P = 0.974$, f: $P = 0.332$, g: $P = 0.872$, h: $P = 0.758$). Response to 3 days of MD was also similar throughout development, with the exception of P35. At this age, bumetanide-, but not vehicle-treated animals showed an OD shift in favor of the ipsilateral (open eye), as shown by lower C/I VEP ratios (post Two Way ANOVA Tukey test, $P < 0.001$). The histograms depict average values ± SEM, whereas circles represent data from single animals. Statistical significance: $*P < 0.05$, $**P < 0.01$, $***P < 0.001$.

Europe PMC Funders Author Manuscripts

Europe PMC Funders Author Manuscripts

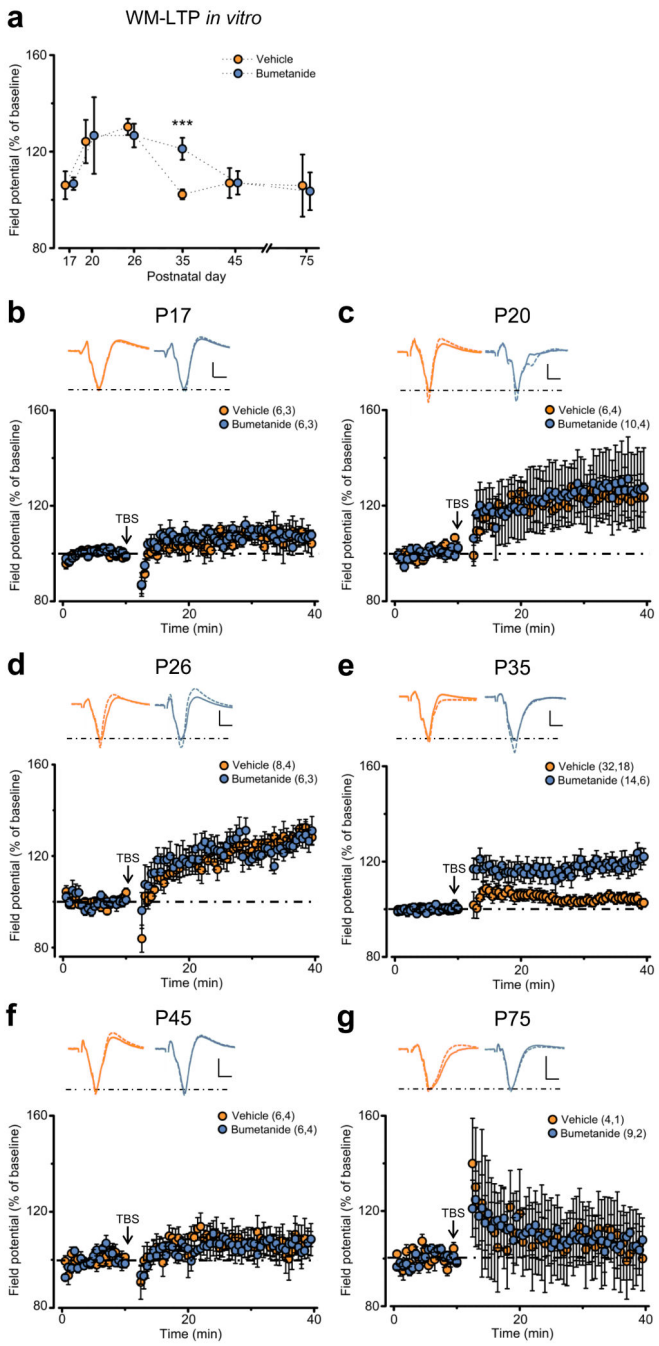

Figure 2.

Early GABAergic interference prolongs critical period plasticity in the visual cortex *in vitro*. (**a**) Average level of plasticity (calculated as the peak amplitude response normalized to the averaged baseline) ± SEM of the amplitude of layer II/III field synaptic potentials after TBS of the WM from experiments performed at different ages and shown in panels (b–g). The level of plasticity was higher in bumetanide-treated animals (blue) than in control vehicles (orange) at P35 (post Two Way ANOVA on ranks Holm-Sidak test, $P < 0.001$), but similar at P17 ($P = 0.969$), P20 ($P = 0.387$), P26 ($P = 0.704$), P45 ($P = 0.860$) and P75 ($P = 0.599$).

(**b–g**) Average time course of the increase in the amplitude of field potentials in vehicle- (orange) and bumetanide-treated animals (blue) at the indicated ages. Insets: average of 10 traces recorded from a slice of a control vehicle (orange) or a bumetanide-treated animal (blue) before (continuous line) and 30 min after TBS (dashed line). Stimulus artifacts have been deleted from traces for clarity. Scale bars: vertical, 0.2 mV; horizontal, 2 ms. Numbers in parentheses: processed slices, animals. Statistical significance: ***$P < 0.001$.

Europe PMC Funders Author Manuscripts

Europe PMC Funders Author Manuscripts

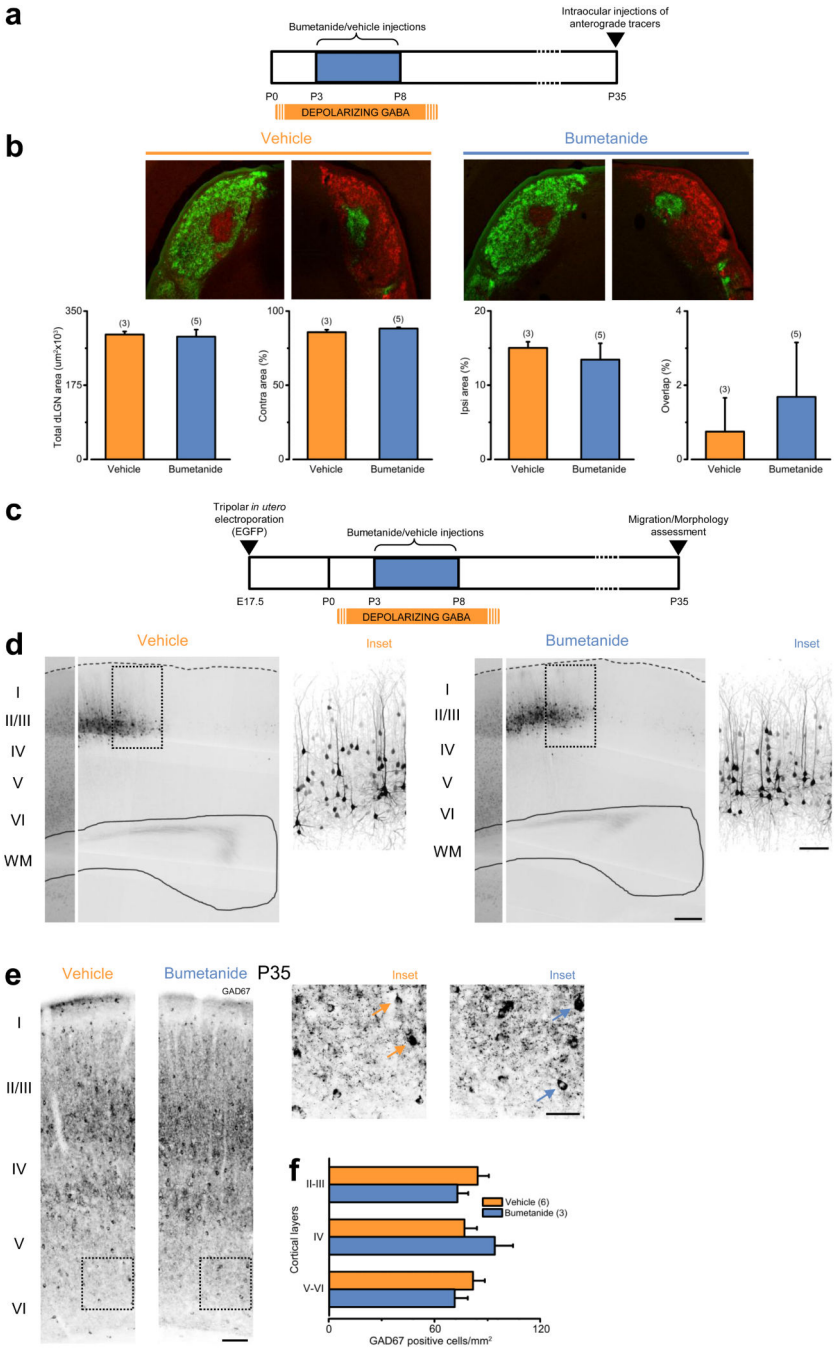

Figure 3.

Early GABAergic interference does not alter the overall structural development of the visual system. (**a**) Schematic cartoon of the experiment for labeling retino-geniculate projections. (**b**) Top: representative coronal sections of left and right sides of dLGN from vehicle- and bumetanide-treated animals after intravitreal injections of green and red cholera toxin beta (CTB) fragment conjugates at P35. Scale bar, 200 μm. Bottom: quantification of total dLGN area, area occupied by contralateral or ipsilateral eye inputs, and overlap of retinal projections from the two eyes revealed no significant differences between the two groups

(Student's *t*-test, $P = 0.831, 0.170, 0.616, 0.666$). The histograms depict average values ± SEM. Numbers in parentheses: processed animals. (**c**) Schematic cartoon of the experiment in panel (d). (**d**) Representative images of EGFP fluorescence in coronal sections of visual cortices at P35 after *in utero* transfection (at E17.5) with pCAG-IRES-EGFP of animals perinatally treated with vehicle (orange) or bumetanide (blue). Scale bar, 200 μm. Insets: higher magnification images from fields as reported on the left. Scale bar, 100 μm. (**e**) Representative images acquired from coronal sections of the visual cortex from vehicle (orange)- and bumetanide-treated animals (blue) at P35 labeled for GAD67. Scale bar, 100 μm. Insets: higher magnification images from fields as reported on the left. Arrows point to examples of GAD67-positive cells. Scale bar, 50 μm. (**f**) Quantification of the density of GAD67-positive cells across cortical layers revealed no significant differences (Two Way ANOVA on ranks, $P = 0.425$). The histogram depicts average ± SEM. Numbers in parentheses: processed animals.

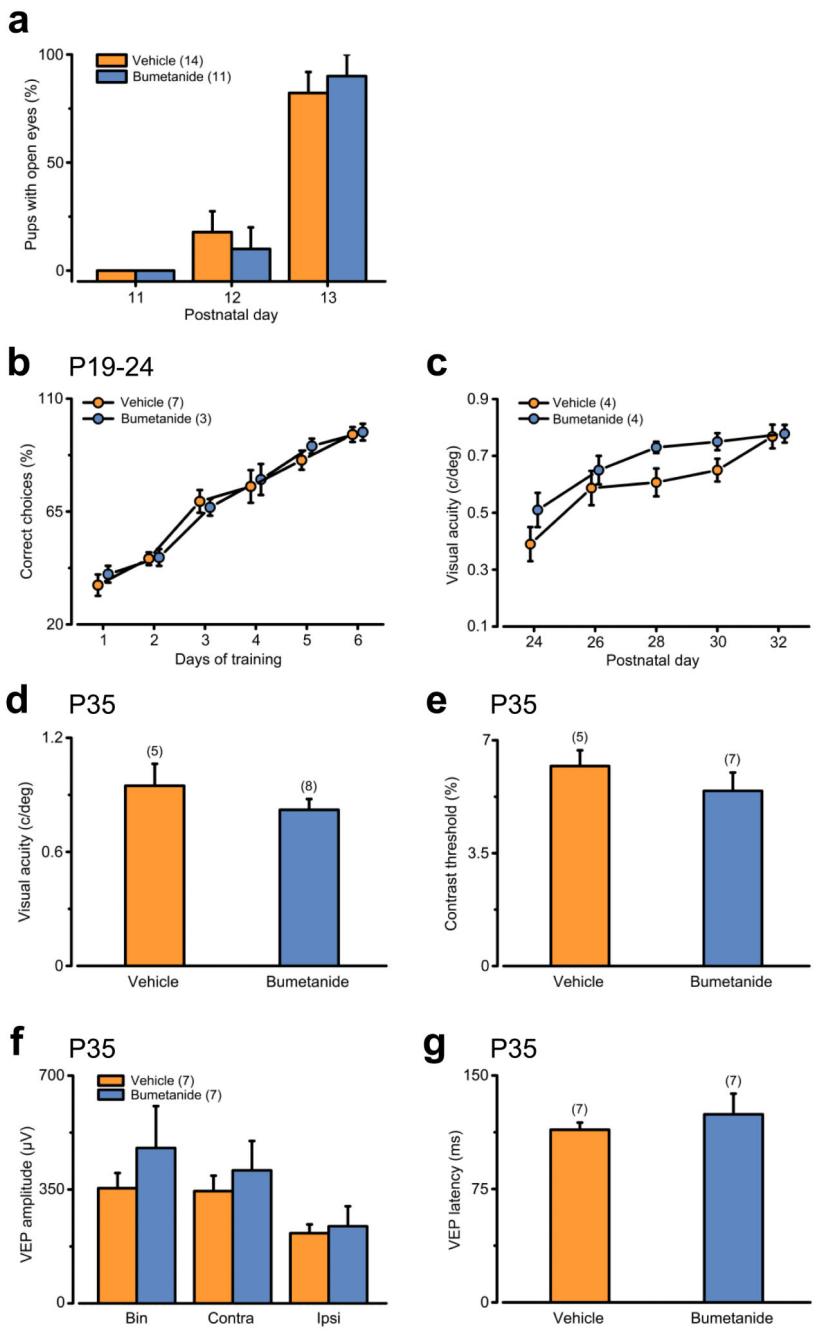

Figure 4.

Early GABAergic interference does not alter the overall functional development of the visual cortex. (**a**) Average percentage (± SEM) of vehicle- (orange) and bumetanide-treated pups (blue) that opened their eyes at the indicated ages. The time of eye opening was similar for three independent litters (χ^2 test, $P = 0.199$). Numbers in parenthesis: analyzed animals. (**b**) The graph reports the performance in learning the Prusky visual water discrimination task (P19-P24) expressed as the % of correct choices ± SEM. The learning curves revealed equivalent visual performances for bumetanide- (blue) and vehicle-treated animals (orange;

Two Way repeated measures ANOVA, $P = 0.968$). (**c**) Development of behavioral visual acuity assessed with the Prusky visual water discrimination task. Two Way repeated measures ANOVA demonstrated a similar age-dependent maturation of visual acuity in bumetanide- and vehicle-treated rats ($P = 0.150$). The histogram depicts average ± SEM. Numbers in parentheses: tested animals. (**d–g**) *In vivo* electrophysiological recordings in the primary visual cortex revealed that bumetanide treatment did not affect the development of basal visual properties such as visual acuity (d), contrast threshold (e), VEP amplitude of binocular, contralateral and ipsilateral responses (f), and VEP latency of binocular responses (g) (Student's *t*-test; d: $P = 0.466$; e: $P = 0.356$; f: $P = 0.385, 0.545, 0.757$; g: $P = 0.993$). The histograms depict average ± SEM. Numbers in parentheses: recorded animals.

Europe PMC Funders Author Manuscripts

Europe PMC Funders Author Manuscripts

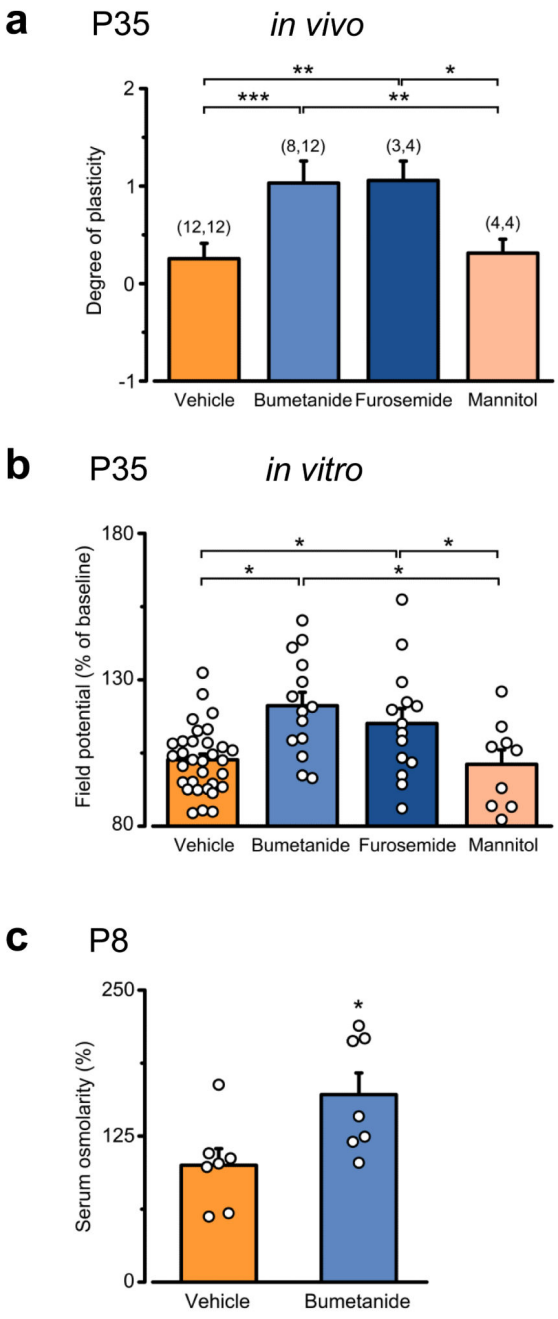

Figure 5.

The effect on visual cortical plasticity upon early bumetanide treatment is due to regulation of cation-Cl^- cotransporters rather than regulation of osmolarity. (**a**) Average ± SEM of the level of OD plasticity in vehicle- (orange), bumetanide- (blue), furosemide- (dark-blue) and mannitol-treated rats (pink) at P35. Higher levels of OD plasticity were found in bumetanide- and furosemide-treated animals (post ANOVA Holm-Sidak test, $P < 0.001$, and $P = 0.004$), but not in mannitol-injected rats ($P = 0.958$). Number in parentheses: recorded animals (nonMD and MD, respectively). (**b**) Average ± SEM and single cases (circles) of

the level of LTP 30 min after TBS in slices from animals treated as in panel (a). Plasticity was greater in bumetanide- (blue) and furosemide-treated animals (dark-blue) than in vehicle-(orange) or mannitol-injected rats (pink; post ANOVA Duncan's test, $P < 0.001$). (**c**) Average serum osmolarity ± SEM measured 10 minutes after acute injection of bumetanide at P8. Osmolarity was increased in bumetanide-treated animals (blue) in comparison to vehicle controls (orange, Student's *t*-test, $P = 0.024$). The histogram depicts average ± SEM, whereas circles represent data from single animals. Statistical significance: $*P < 0.05$, $**P < 0.01$, $***P \leq 0.001$.

Europe PMC Funders Author Manuscripts

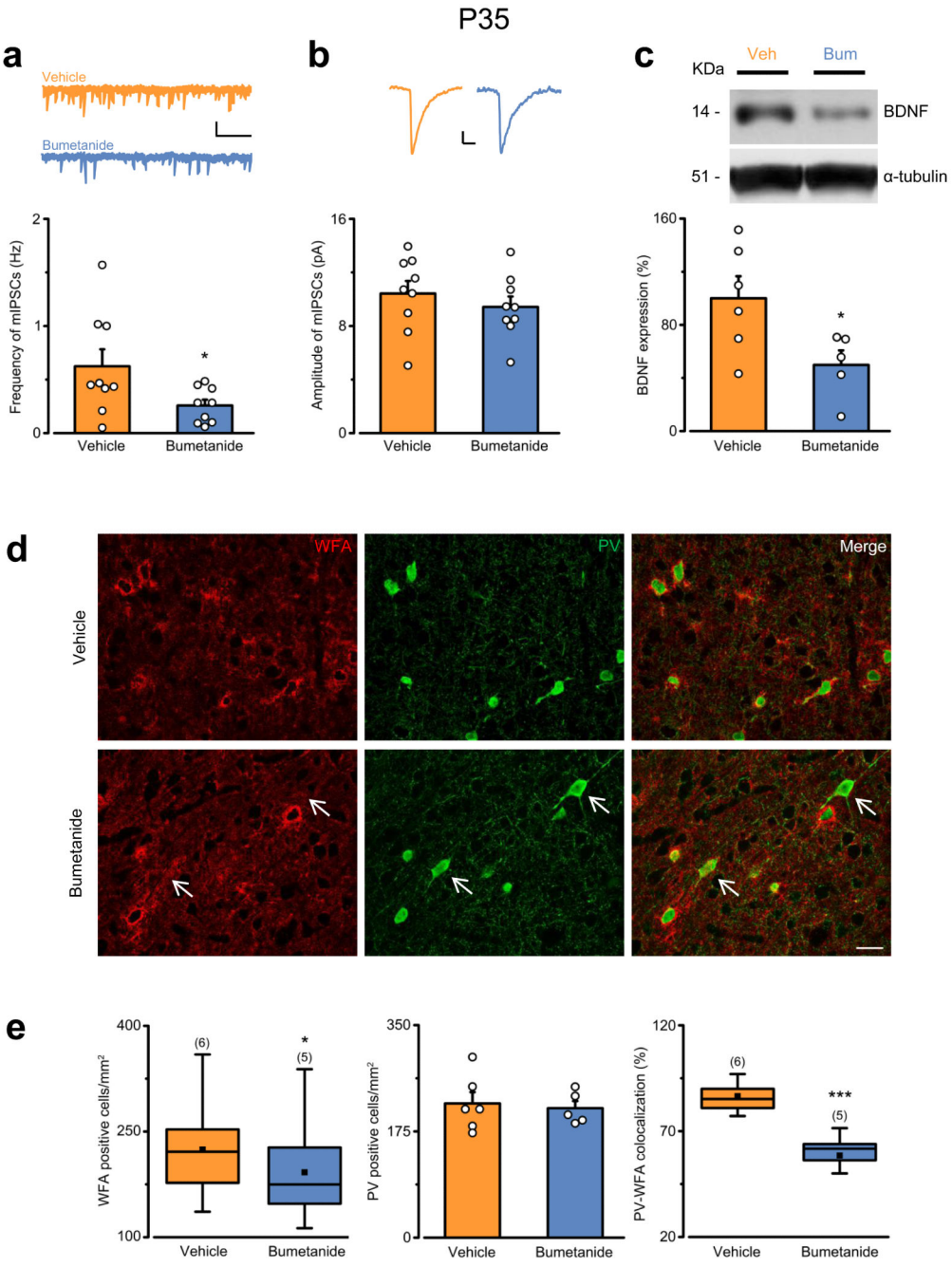

Figure 6.

Early GABAergic interference decreases the cortical inhibitory tone, reduces BDNF expression, and impairs the maturation of PNNs in adulthood. (**a**) Top: mIPSCs in P35 animals treated perinatally with vehicle (orange) or bumetanide (blue). Bottom: quantification of mIPSC frequency (Student's *t*-test, $P = 0.045$). The histogram represents average ± SEM, whereas circles indicate data from single cells. Scale bars: vertical 10, pA; horizontal, 2 s. (**b**) Top: average traces of 50 mIPSC events from vehicle- (orange) and bumetanide-treated animals (blue). Bottom: quantification of mIPSC amplitudes (Student's

Europe PMC Funders Author Manuscripts

t-test, $P = 0.426$). The histogram depicts average ± SEM, whereas circles indicate data from single cells. Scale bars: vertical, 2 pA; horizontal, 10 ms. (**c**) Cropped images of immunoblotting for BDNF on protein extracts from P35 visual cortices of vehicle- (orange) or bumetanide-treated animals (blue). α-tubulin was used as internal standard. Full-length blots are presented in Supplementary Figure 11a. Bottom: average ± SEM and data from single animals (circles) (Student's *t*-test, $P = 0.039$). (**d**) Coronal sections of the visual cortex from P35 vehicle- and bumetanide-treated animals double-labeled for perineuronal nets (PNNs, WFA, red) and parvalbumin (PV, green). Arrows indicate PV-positive cells not surrounded by PNNs. Scale bar, 20 μm. (**e**) Quantification of the density of PNN-positive cells (left; Mann-Whitney rank sum test, $P = 0.019$) and PV-positive cells (middle; Student's *t*-test, $P = 0.511$), and percentage of PV-PNN-double-labeled cells (right; Mann-Whitney rank sum test, $P < 0.001$). (). The data in the left and right panels are summarized by a box chart, whereas the histogram in the middle panel represents average ± SEM. Statistical significance: $*P < 0.05$, $***P \leq 0.001$.

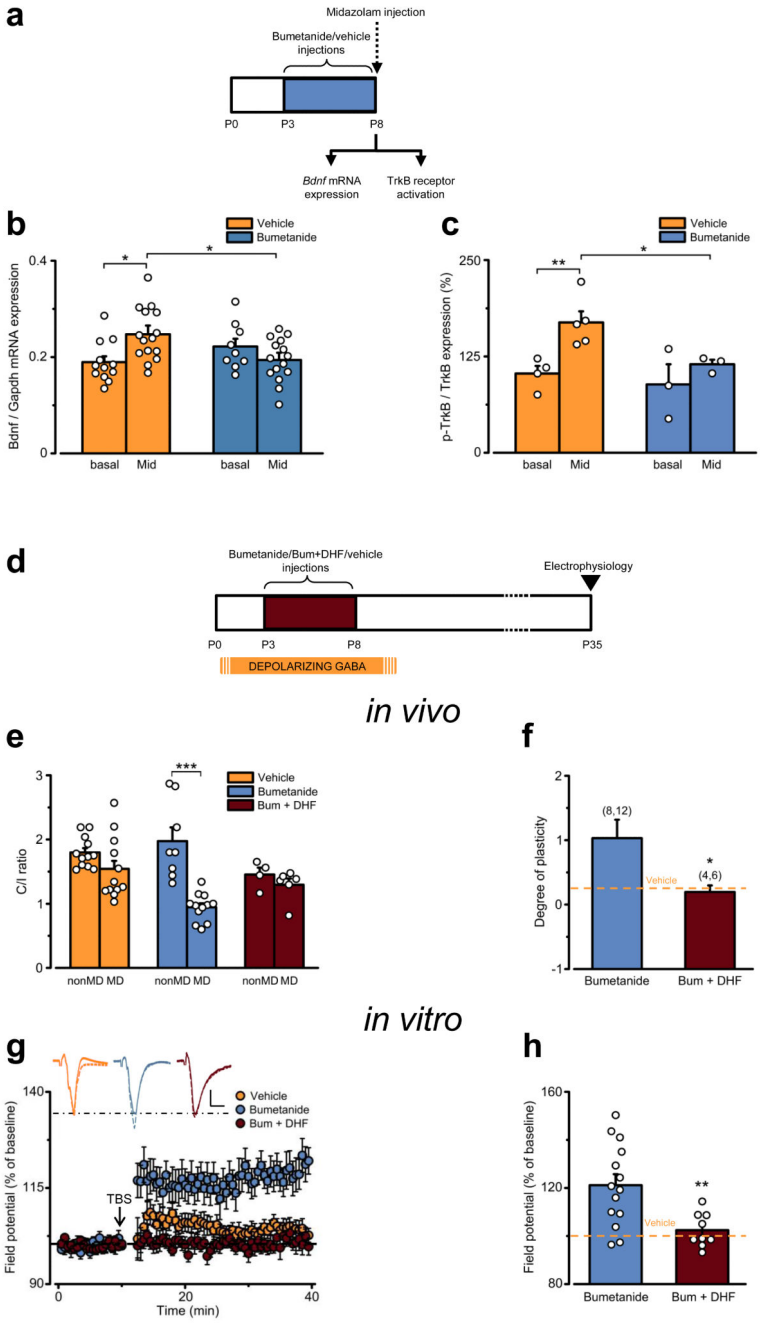

Figure 7.

DHF treatment during early GABAergic interference rescues bumetanide-induced effect on plasticity. (**a**) Cartoon of the experimental protocol. (**b**) *BDNF* mRNA expression in P8 vehicle- (orange) and bumetanide-treated pups (blue) in basal condition or after induction by i.p. injection of $GABA_A$ receptor agonist Midazolam. *Gapdh* was used as internal standard. Two Way ANOVA showed that bumetanide treatment blocked (post Tukey test, $P = 0.004$) the Midazolam-induced increase (post Tukey test, $P = 0.003$) of *Bdnf* mRNA expression. The histogram depicts average ± SEM, circles indicate single data. (**c**) Ratio of p-TrkB/TrkB

protein expression in P8 vehicle- (orange) and bumetanide-treated pups (blue) in basal condition or after Midazolam induction. Two Way ANOVA showed that bumetanide treatment blocked (post Tukey test, $P = 0.029$) the Midazolam-induced increase (post Tukey test, $P = 0.006$) of p-TrkB/TrkB protein expression. The histogram depicts average ± SEM, circles indicate single data. (**d**) Cartoon of the experimental protocol. (**e**) C/I VEP ratios in P35 animals perinatally treated with vehicle- (orange), bumetanide- (blue), or bumetanide +DHF (dark red), non-deprived (nonMD) or monocularly deprived (MD). Two Way ANOVA revealed that plasticity in bumetanide+DHF-treated animals was negligible ($P = 0.505$). The histogram depicts average ± SEM, circles indicate single animals. (**f**) Average degree of OD plasticity ± SEM for data in (e) (Student's *t*-test, $P = 0.030$). The dotted orange line represents the average level of plasticity in vehicle-treated rats. Number in parentheses: recorded animals (nonMD and MD, respectively). (**g**) Average time-course of WM-LTP in P35 vehicle-, bumetanide-, or bumetanide+DHF-treated animals. Insets: Average of 10 traces recorded from vehicle- (orange), bumetanide- (blue), or bumetanide +DHF-treated animal (dark red) before (continuous line) and 30 min after TBS (dashed line). Scale bars: vertical, 0.2 mV; horizontal, 2 ms. (**h**) Data from single slices (circles) recorded in panel (g) and average ± SEM of the plasticity level (normalized to controls, dotted orange line; Student's *t*-test, $P = 0.005$). Statistical significance: $^{*}P < 0.05$, $^{**}P < 0.01$, $^{***}P < 0.001$.

Europe PMC Funders Author Manuscripts

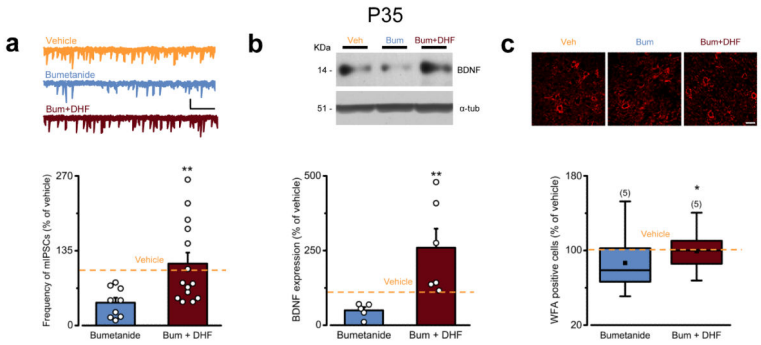

Figure 8.

DHF treatment during early GABAergic interference rescues bumetanide-induced effect on regulators of plasticity. (**a**) Top: representative mIPSCs of P35 neurons from vehicle- (orange), bumetanide- (blue), or bumetanide+DHF-treated animals (dark red). Bottom: quantification of mIPSC frequency (normalized to vehicle average; Student's *t*-test, $P = 0.012$). The histogram depicts mean ± SEM, whereas circles indicate data from single cells. Scale bars: vertical, 10 pA; horizontal, 5 s. The orange dotted line indicates average mIPSCs frequency in vehicle-treated rats for comparison. (**b**) Top: Cropped images of representative immunoblotting for BDNF on protein extracts from P35 visual cortices of vehicle- (orange), bumetanide- (blue) and bumetanide+DHF-treated animals (dark red). α-tubulin was used as internal standard. Full-length blots are presented in Supplementary Figure 11b. Bottom: quantification of BDNF levels in bumetanide- (blue) and bumetanide+DHF-treated animals (dark red) normalized to vehicle average (Mann Whitney Rank Sum Test, $P = 0.004$). The histogram represents average ± SEM and circles indicate data from single animals. The orange dotted line indicates BDNF level in vehicle-treated rats. (**c**) Top: representative images of PNNs from P35 coronal sections of the visual cortex from vehicle- (orange), bumetanide- (blue) and bumetanide+DHF-treated animals (dark red). Scale bar, 20 μm. Bottom: quantification of the density of PNN-positive cells (normalized to the median of vehicle controls; Student's *t*-test $P = 0.019$). Data are summarized by a box chart. The orange dotted line represents the median density of WFA positive cells in vehicle-treated rats for comparison. Statistical significance: $*P < 0.05$, $**P \leq 0.01$.